

# MaLoRA: Gated Modality LoRA for Key-Space Alignment in Multimodal LLM Fine-Tuning

Xinhan Zheng\*  
xinhanzheng@mail.ustc.edu.cn  
University of Science and Technology  
of China  
Hefei, China

Huyu Wu\*  
wuhuyu25@mails.ucas.ac.cn  
University of Chinese Academy of  
Sciences  
Beijing, China

Xueting Wang\*  
wangxueting@mail.ustc.edu.cn  
University of Science and Technology  
of China  
Hefei, China

Duo Su  
sduo@mail.tsinghua.edu.cn  
Tsinghua University  
Beijing, China

Haiyun Jiang<sup>†</sup>  
haiyunjiang@sjtu.edu.cn  
Shanghai Jiao Tong University  
Shanghai, China

## Abstract

Multimodal large language models (MLLMs) often exhibit *text-centric bias* under joint image–text inputs, over-relying on textual signals and under-using visual evidence. We analyze decoder self-attention and observe a persistent cross-modal misalignment in the attention *key space*, where visual and text keys form separated distributions consistent with attention favoring text tokens. Motivated by this finding, we propose **Modality Alignment LoRA (MaLoRA)**, a fine-tuning framework that targets key-space misalignment via three designs: Gated Modality LoRA (GML) for modality-conditioned key adaptation, multi-kernel maximum mean discrepancy (MMD) for cross-modal distribution alignment, and Gram reference regularization to preserve within-modality structure during alignment. Extensive experiments across three MLLM backbones and diverse benchmarks demonstrate that MaLoRA reduces key-space divergence and yields measurable improvements in downstream performance.

## Keywords

Multimodal Large Language Models, Vision-Language Fine-tuning, Text-centric Bias

## 1 Introduction

Multimodal large language models (MLLMs) have demonstrated strong performance across vision–language tasks by integrating visual and textual signals within a unified generative framework. Ideally, such models should dynamically balance modalities according to task-relevant evidence. However, empirical observations reveal a systematic deviation: under joint image–text inputs, MLLMs exhibit a pronounced preference for textual information, often neglecting visual cues even when they are essential for correct reasoning. This **text-centric bias** persists across architectures, datasets, and training regimes, suggesting that it reflects a fundamental property of multimodal generative modeling rather than a superficial artifact of data or optimization.

Existing approaches primarily address this issue through data curation, alignment objectives, architectural modifications, or inference-time heuristics [2, 9, 12, 24, 28]. However, the model-internal mechanism underlying text-dominant behavior remains insufficiently understood. This gap motivates us to investigate how modality imbalance emerges within the attention computation of MLLMs.

In this work, we argue that text-centric bias originates from a structural property of decoder self-attention in MLLMs: **cross-modal misalignment in the attention key space**. Formally, although visual and textual tokens are projected through shared key matrices, their resulting key representations follow distinct distributions.

Since decoder queries are shaped predominantly by language-model pretraining, they align more naturally with textual key distributions, yielding systematically higher similarity scores with text tokens than visual. This induces a biased attention allocation mechanism that is intrinsic to the geometry of the key space rather than the semantics of the input.

To examine the hypothesis that text-centric bias in MLLMs is linked to cross-modal misalignment in the attention key space, we conduct a multi-layer analysis of key representations in several representative MLLMs. By visualizing key distributions and quantifying their divergence using distributional metrics, we demonstrate that visual and textual keys form persistently separated manifolds across layers and models. Moreover, the magnitude of cross-modal divergence significantly exceeds within-modality variation, establishing key-space misalignment as a persistent and fundamental phenomenon. These observations suggest that modality bias is not merely an optimization artifact but a consequence of distributional mismatch in the latent space that governs attention computation.

This perspective reframes multimodal bias mitigation as a *distribution alignment problem in the attention key space*. However, directly aligning visual and textual keys raises two theoretical challenges. First, visual and textual tokens require modality-specific adaptation directions, making shared parameter updates insufficient and potentially conflicting. Second, naive alignment risks collapsing or distorting the intrinsic geometry of modality-specific representations, thereby degrading the reasoning capacity of models. Therefore, an effective intervention must simultaneously enable modality-conditioned adaptation and preserve structural properties of the original representation space.

\*Both authors contributed equally to this research.

<sup>†</sup>Corresponding author.

To address these challenges, we propose **MaLoRA**, a fine-tuning framework that targets key-space misalignment. MaLoRA introduces (i) **Gated Modality LoRA**, which decomposes key adaptation into modality-specific low-rank subspaces, (ii) **distribution-level alignment** via multi-kernel maximum mean discrepancy to reduce cross-modal divergence, and (iii) **structure-preserving regularization** based on Gram reference to constrain geometric drift during alignment. Together, these components provide a principled mechanism for reshaping the key-space geometry while maintaining representational integrity, without altering the inference process.

Extensive experiments across multiple MLLM backbones and benchmarks show that MaLoRA consistently reduces cross-modal key divergence and improves performance, particularly in tasks that require genuine visual grounding. Beyond empirical gains, our analysis highlights the attention key space as a previously underexplored locus of multimodal bias and offers a theoretically grounded framework for understanding and mitigating modality imbalance in generative multimodal models.

Our contributions are as follows:

- Starting from standard self-attention, we connect *text-centric bias* to the attention *key space* and identify cross-modal key misalignment as a key contributing factor. We hypothesize that cross-modal key distribution misalignment correlates with a systematic preference for text tokens, and support it with multi-layer visualization and divergence measurements across backbones and benchmarks.
- We propose **MaLoRA**, a fine-tuning framework that directly intervenes on key-space misalignment: **Gated Modality LoRA (GML)** enables modality-conditioned key adaptation, and **MMD alignment** together with **Gram reference** structure preservation reduces cross-modal gaps while avoiding excessive distortion of representation geometry.
- We validate MaLoRA on evaluations spanning diverse tasks and datasets. The method consistently reduces distribution divergence between visual and textual representations and improves downstream performance.

## 2 Related Work

### 2.1 Modality bias and text-centric bias in MLLMs

MLLMs often exhibit modality imbalance in generative tasks: they rely on linguistic priors over visual evidence and may generate hallucinated content when visual cues are weak or not aligned with question-critical evidence [9, 12, 24, 28]. Recent work has begun to systematically characterize this *text dominance* phenomenon. Wu et al. [27] analyze its prevalence across multiple non-text modalities (images, videos, audio) and proposes quantitative metrics to assess the degree of modality dominance. Meanwhile, Park et al. [19] argues that benchmarks contain limited cases that truly require multimodal fusion, which amplifies unimodal bias. Liu et al. [13] discusses modality imbalance under alignment and preference optimization and proposes optimization frameworks for modality balance. Complementary to these perspectives on phenomenon, data, and training strategy, we further analyze the internal mechanism

of text dominance from the self-attention *key space* distribution, and show that the out-of-distribution nature of visual keys can systematically affect attention allocation and generation behavior.

### 2.2 Structural or inference-time mitigation methods

Existing mitigation strategies mainly operate either by modifying multimodal fusion and training signals or by suppressing hallucination at inference time.

To address weakened visual evidence usage and hallucinations caused by text dominance, one line of work modifies fusion architectures or training signals to increase the contribution of visual information in generation. For example, LACING introduces dual-branch attention for vision and text at the attention layer, combined with soft visual prompts to reduce text-centric bias [30]. However, LACING operates in the full-parameter multimodal alignment setting, requiring complete two-stage retraining of the model from the LLM backbone (e.g., 558K pretraining + 665K instruction tuning on  $8 \times A100$  GPUs), and further relies on a contrastive decoding strategy at inference time. In contrast, MaLoRA targets the parameter-efficient fine-tuning regime, adapting pre-trained instruct models to downstream tasks with only lightweight LoRA updates and standard autoregressive decoding. The two approaches are thus complementary, addressing text-centric bias at different stages of the MLLM lifecycle. Unlike MoE architectures that primarily expand capacity via dynamic routing, GML introduces modality-specific LoRA branches within  $k_{proj}$  as separate adaptation interfaces for visual and textual tokens.

Another line of work keeps model parameters fixed and suppresses erroneous tokens triggered by linguistic priors at inference time via contrastive decoding or probabilistic penalties. VCD reduces language priors by contrasting output distributions between the original image and a perturbed image [12]. OPERA applies an over-trust penalty in beam search based on aggregated attention patterns and performs backtracking to re-rank candidates [9]. ICD contrasts the distributions under standard instructions and “perturbed instructions” to offset hallucinated concepts [26]. CATCH further adopts adaptive token-level contrast to mitigate accumulated hallucinations in open-ended generation [10].

Overall, these methods intervene at the architecture or decoding stage. In contrast, training-time constraints that directly target cross-modal discrepancy in the decoder self-attention *key space* remain relatively underexplored. In many cases, inference-time methods introduce extra decoding steps or additional forward passes, and they do not directly alter representation misalignment. We instead intervene during fine-tuning by constraining cross-modal gaps in the attention *key space*, while keeping inference unchanged.

### 2.3 Cross-modal alignment and distribution alignment

Cross-modal representation alignment and distribution matching are common approaches in multimodal learning and domain generalization/adaptation. They include optimal-transport (OT) based structure-preserving alignment [4] and kernel-based statistical distances such as maximum mean discrepancy (MMD) [7, 23]. In addition, Song et al. [22] studies semi-supervised alignment from a

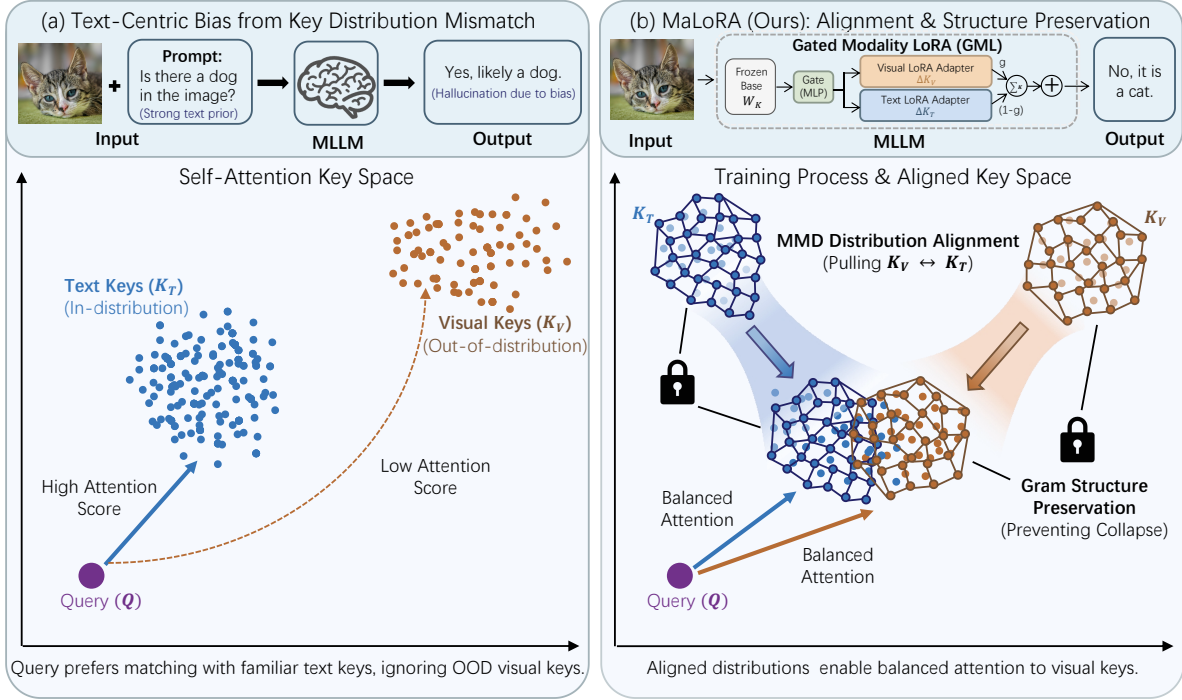


Figure 1: The MaLoRA framework addressing *text-centric bias* in MLLMs.

distributional perspective and discusses training paradigms that improve cross-modal semantic consistency under weak pairing or limited alignment data. Existing distribution alignment work mainly targets representation learning and adaptation settings. We introduce distribution alignment into the attention key space of MLLMs to address their modality-specific bias mechanism.

### 3 Key-Space Misalignment

Under image–text inputs, MLLMs often over-rely on textual information during generation, exhibiting *text-centric bias*. **We hypothesize that this phenomenon is not solely due to data composition or alignment objectives, but may stem from key-space distribution misalignment in decoder self-attention.** We recall the standard self-attention formulation:

$$\text{Attn}(\mathbf{Q}, \mathbf{K}, \mathbf{V}) = \text{softmax}\left(\frac{\mathbf{Q}\mathbf{K}^\top}{\sqrt{d}}\right)\mathbf{V}, \quad (1)$$

where  $\mathbf{Q}$ ,  $\mathbf{K}$ , and  $\mathbf{V}$  denote the query, key, and value matrices, respectively, and  $d$  is the per-head dimension. At the token level, the attention score between a query  $\mathbf{q}_i$  and a key  $\mathbf{k}_j$  is determined by their scaled dot product  $\mathbf{q}_i^\top \mathbf{k}_j / \sqrt{d}$ . In contrast, visual tokens are projected from a vision encoder and concatenated with text tokens, inheriting a cross-modal gap before entering the decoder. At each layer, both visual and textual keys are produced from their hidden states through a shared key projection  $\mathbf{W}_k$ . Despite sharing the projection,  $\mathbf{K}_{\text{vis}}$  and  $\mathbf{K}_{\text{text}}$  may still exhibit substantial distribution differences in the key space. As a result,  $\mathbf{q}$  may be better aligned with  $\mathbf{k}^{\text{text}}$ , yielding higher similarity scores and attention allocation bias toward text tokens.

To test this hypothesis, we perform *key-space probing*, extracting keys and analyzing their geometry and divergence, on several decoder layers of representative MLLMs. Given joint image-text inputs, we extract the sets of visual and textual key vectors  $\mathbf{k}^{\text{vis}}$ ,  $\mathbf{k}^{\text{text}}$  from target layers and mask padding tokens. First, we visualize the geometry of the two key sets on selected layers using t-SNE. Second, we quantify cross-modal discrepancy using distributional measures (primarily MMD), comparing  $P(\mathbf{K}^{\text{vis}})$  and  $P(\mathbf{K}^{\text{text}})$  and contrasting them with within-modality baselines computed from split subsets.

Qualitatively, the base model shows a clear separation between visual and textual keys in the t-SNE reduced space across both benchmarks (Figure 2, left), suggesting an inherent cross-modal key-space discrepancy. With our method, the two distributions become noticeably closer and more overlapping, indicating that this discrepancy is substantially alleviated. The layer-wise modality gap analysis (Figure 2, right) further confirms that this separation persists across layers in the base model, while MaLoRA consistently reduces the gap throughout the network on both Qwen3-VL-8B (MMBench-EN) and Qwen2.5-VL-7B (MMMU), suggesting that visual keys are progressively better integrated into the textual key distribution.

This key space separation affects attention computation. From Eq. (1), when  $\mathbf{q}$  is better aligned with the textual key distribution,  $\mathbf{q}^\top \mathbf{k}^{\text{text}}$  tends to be larger, while  $\mathbf{q}^\top \mathbf{k}^{\text{vis}}$  tends to be smaller and is further down-weighted after softmax. Consequently, even when visual tokens contain question-critical information, the model is more likely to allocate attention to text tokens or previously generated context, resulting in insufficient use of image evidence when

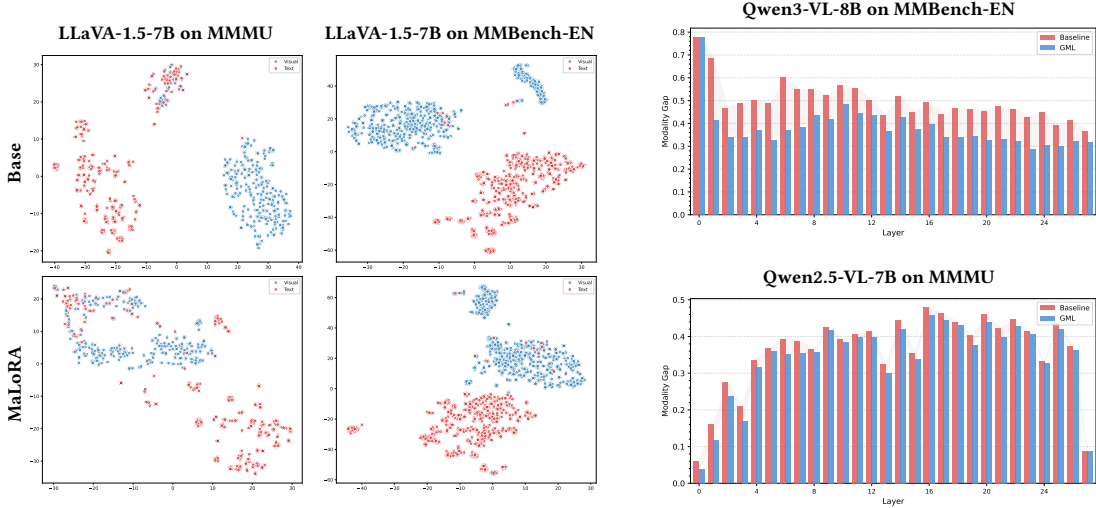


Figure 2: Left: t-SNE visualization of hidden representations for Base and MaLoRA on LLaVA-1.5-7B, evaluated on MMMU (left column) and MMBench-EN (right column). Right: Representation gap analysis for Qwen3-VL-8B on MMBench-EN (top) and Qwen2.5-VL-7B on MMMU (bottom).

generating the answer. These results suggest that visual–textual key misalignment is an important factor in *text-centric bias*.

## 4 Method

To mitigate *text-centric bias* in MLLMs under joint image-text inputs, we propose the **MaLoRA** framework. It consists of two core components: 1) **Architecture**: GML adds modality-specific LoRA branches to the decoder self-attention  $k_{proj}$  and uses a lightweight gate to enable modality-conditioned key adaptation. 2) **Regularization**: we add training-time constraints, including MK-MMD for distribution alignment and Gram-matrix regularization for structure preservation, to encourage a modality-balanced *key space* without changing inference.

Following the self-attention formulation in Eq. (1), for the decoder at layer  $l$ , the input hidden states are  $\mathbf{H}^{(l)}$ . We assume that  $\mathbf{K}_{vis}^{(l)}$  and  $\mathbf{K}_{text}^{(l)}$  exhibit persistent misalignment in the key space, which is associated with decoder queries preferentially matching text tokens.

### 4.1 Gated Modality LoRA (GML)

To enable token-wise modality conditioning, we extend  $k_{proj}$  with a gated two-branch LoRA design. Given input  $\mathbf{H}^{(l)}$ , the resulting key representation is:

$$\mathbf{K}^{(l)} = \mathbf{H}^{(l)} \mathbf{W}_k^{(l)} + \alpha \cdot \left[ g \cdot \Delta \mathbf{K}_{vis}^{(l)} + (1 - g) \cdot \Delta \mathbf{K}_{text}^{(l)} \right], \quad (2)$$

where  $\Delta \mathbf{K}_{vis}$  and  $\Delta \mathbf{K}_{text}$  denote the visual and textual LoRA branches, respectively. The gate  $g \in [0, 1]$  is predicted by a lightweight gating network:

$$g = \sigma \left( \text{MLP}(\mathbf{H}^{(l)}) \right), \quad (3)$$

where  $\sigma$  is the sigmoid activation. To ensure precise modality-specific routing, we supervise the gating network with a token-level

binary cross-entropy loss  $\mathcal{L}_{gate}$  using known modality labels from the input packing:

$$\mathcal{L}_{gate}^{(l)} = - [y \log(g) + (1 - y) \log(1 - g)], \quad (4)$$

where  $y$  is the modality ground truth for the current token. During training, we adopt a linear annealing schedule that transitions the gating mechanism from early label guidance to fully model-predicted gating.

### 4.2 Distribution Alignment via Multi-kernel MMD

MaLoRA uses multi-kernel maximum mean discrepancy (MK-MMD) to reduce the distribution gap between visual and textual keys. For layer  $l$ , we define the alignment loss as:

$$\mathcal{L}_{mmd}^{(l)} = \text{MMD}^2 \left( \mathcal{K}_{vis}^{(l)}, \mathcal{K}_{text}^{(l)} \right). \quad (5)$$

Given a kernel family  $\{k_m\}$ , the multi-kernel form is  $k(\mathbf{a}, \mathbf{b}) = \sum \alpha_m k_m(\mathbf{a}, \mathbf{b})$ . Minimizing this term reduces cross-modal distribution mismatch in the key space.

### 4.3 Structure Preservation via Gram Reference Regularization

To prevent alignment from inducing excessive geometric drift, we introduce a Gram-based regularizer that preserves the relative geometry of the original key representations. Let  $\mathbf{A}_\theta^{(l)}$  denote the set of visual keys at layer  $l$  in the current model. Its Gram matrix is defined as  $\mathbf{G}(\mathbf{A}) = \mathbf{A} \mathbf{A}^\top$ . The structure preservation loss is:

$$\mathcal{L}_{gram}^{(l)} = \left\| \mathbf{G}(\mathbf{A}_\theta^{(l)}) - \mathbf{G}(\mathbf{A}_{\theta_{ref}}^{(l)}) \right\|_F^2. \quad (6)$$

This constraint preserves correlation structure in a second-order sense, helping that the model retains its original reasoning capability while mitigating bias.

**Table 1: Key-space divergence at decoder layer 1 for LLaVA-1.5-7B, Qwen2.5-VL-7B, and Qwen3-VL-8B on MMBench-EN and MMMU (10-option). MMD and JS show Image vs. Text consistently larger than Image vs. Image and Text vs. Text. This gap aligns with a persistent separation between visual and textual keys in the projected embedding space.**

(a) MMD						(b) JS							
Comparison	LLaVA-1.5-7B		Qwen2.5-VL-7B		Qwen3-VL-8B		Comparison	LLaVA-1.5-7B		Qwen2.5-VL-7B		Qwen3-VL-8B	
	MMB-EN	MMMU	MMB-EN	MMMU	MMB-EN	MMMU		MMB-EN	MMMU	MMB-EN	MMMU	MMB-EN	MMMU
Image vs. Text	<b>0.94</b>	<b>0.95</b>	<b>0.57</b>	<b>0.71</b>	<b>0.76</b>	<b>0.76</b>	Image vs. Text	<b>0.82</b>	<b>0.84</b>	<b>0.86</b>	<b>0.86</b>	<b>0.72</b>	<b>0.66</b>
Image vs. Image	0.01	0.01	0.01	0.01	0.01	0.09	Image vs. Image	0.04	0.03	0.04	0.04	0.04	0.09
Text vs. Text	0.02	0.02	0.01	0.07	0.04	0.03	Text vs. Text	0.14	0.10	0.14	0.14	0.15	0.15

### 4.4 Overall Objective

The final training objective  $\mathcal{L}$  combines the task loss, distribution alignment loss, structure preservation loss, and gate supervision loss:

$$\mathcal{L} = \mathcal{L}_{\text{task}} + \lambda_{\text{mmd}} \sum_{l \in \mathcal{L}} \mathcal{L}_{\text{mmd}}^{(l)} + \lambda_{\text{gram}} \sum_{l \in \mathcal{L}} \mathcal{L}_{\text{gram}}^{(l)} + \lambda_{\text{gate}} \sum_{l \in \mathcal{L}} \mathcal{L}_{\text{gate}}^{(l)} \tag{7}$$

Here  $\lambda_{\text{mmd}}$ ,  $\lambda_{\text{gram}}$ , and  $\lambda_{\text{gate}}$  are hyperparameters. At inference time, GML predicts token-wise gates on the fly, applying modality-conditioned key adaptation without changing the decoding procedure.


## 5 Experiments

### 5.1 Experimental Setup

*Models and Training Settings.* We evaluate MaLoRA on three representative instruction-tuned MLLMs: LLaVA-1.5-7B-Instruct, Qwen2.5-VL-7B-Instruct, and Qwen3-VL-8B-Instruct. These backbones cover different multimodal LLM families and provide a representative testbed for parameter-efficient adaptation. All models follow the standard vision-language input format, in which an image is encoded into visual tokens and concatenated with text tokens for decoding. Unless noted otherwise, we use each model’s default vision encoder configuration, visual token budget, and pre-processing pipeline. We compare four training settings: Base, LoRA, QLoRA, and MaLoRA. For a fair comparison, all methods use the same training data, optimization schedule, batch size, and number of training epochs or steps. Additional implementation details are provided in the appendix.


*Benchmarks and Task Taxonomy.* We evaluate on a diverse benchmark suite spanning seven capability groups (Table 2): **General Understanding** (MMBench-EN [14]), **Expert Reasoning** (MMMU [29], SimpleVQA [5], MMStar [3]), **Math Reasoning** (WeMath [20], MathVision [25]), **OCR QA** (OCRVQA [18], TextVQA [21], ST-VQA [1]), **Structured QA** (DocVQA [17], ChartQA [16]), **GUI Grounding** (RICO-ScreenQA [8]), and **Domain-Specific** (VQA-RAD [11], RSVQA [15]). This taxonomy is intended to stress-test *text-centric bias* in settings where visual evidence is essential. In **OCR**, **Structured**, and **GUI** tasks, the decisive signal comes directly from the image, such as rendered text, layout, or structural cues, so linguistic shortcuts are especially fragile. **Domain-Specific**

benchmarks further introduce substantial distribution shifts, including remote sensing and radiology, which can increase reliance on textual priors.


 <image> == = Egypt and Palestine == =

-----




What do the words say?  
Output exactly two parts: 1. Answer: <short answer>  
2. Reasoning: <one brief sentence>.



----->



The answer is here.

-  Qwen3-VL-8B
  - 1. Answer: **Egypt and Palestine**
  - 2. Reasoning: The text directly states "Egypt and Palestine" as the words being asked about. ✗
-  Fintune with LoRA
  - 1. Answer: **Egypt and Palestine**
  - 2. Reasoning: The text in the image clearly reads "Egypt and Palestine". ✗
-  Fintune with MaLoRA
  - 1. Answer: 208
  - 2. Reasoning: The number 208 is clearly visible on the side of the boat in the image. ✔

**Figure 3: Case study on image-text irrelevant data. MaLoRA alleviates text-centric bias, enabling the model to rely on visual evidence instead of misleading text, while LoRA and the Base model fail to do so.**

### 5.2 Main Results

Table 2 reports per-benchmark results for all three backbones under four training settings: **Base** (no task fine-tuning), **LoRA**, **QLoRA**, and **Ours** (MaLoRA).

*Overall trend.* Across 14 benchmarks covering seven capability groups, MaLoRA gives the strongest overall performance on all three backbones. It achieves the best or tied-best result on all 42 backbone-benchmark pairs. The advantage is especially clear

**Table 2: Per-benchmark results on three instruct models (LLaVA-1.5-7B, Qwen2.5-VL-7B, and Qwen3-VL-8B) under four training settings (Base, LoRA, QLoRA, and Ours), where Base denotes no task fine-tuning. Data reports the number of training examples used for fine-tuning on each benchmark. Benchmarks are grouped by capability categories, covering a broad and diverse evaluation suite. For each dataset and model, the best result among the four settings is shown in bold.**

Category	Benchmark	Data	LLaVA-1.5-7B				Qwen2.5-VL-7B				Qwen3-VL-8B			
			Base	LoRA	QLoRA	Ours	Base	LoRA	QLoRA	Ours	Base	LoRA	QLoRA	Ours
Gen.Understand	MMBench-EN	3.5k	72.52 $\pm$ 0.23	80.25 $\pm$ 0.35	80.95 $\pm$ 0.00	<b>82.80<math>\pm</math>0.35</b>	90.30 $\pm$ 0.27	90.18 $\pm$ 0.24	88.91 $\pm$ 0.07	<b>92.84<math>\pm</math>0.24</b>	91.34 $\pm$ 0.40	92.03 $\pm$ 0.12	89.03 $\pm$ 0.20	<b>93.53<math>\pm</math>0.29</b>
Expert Reasoning	SimpleVQA	1.8k	14.16 $\pm$ 0.00	18.20 $\pm$ 0.58	19.32 $\pm$ 0.44	<b>19.78<math>\pm</math>0.46</b>	35.51 $\pm$ 0.13	37.98 $\pm$ 0.51	35.51 $\pm$ 0.55	<b>39.33<math>\pm</math>0.25</b>	37.98 $\pm$ 0.71	38.65 $\pm$ 0.76	36.63 $\pm$ 0.76	<b>39.78<math>\pm</math>0.38</b>
	MMStar	1.2k	36.67 $\pm$ 1.15	36.67 $\pm$ 1.02	37.33 $\pm$ 0.88	<b>37.35<math>\pm</math>0.51</b>	65.67 $\pm$ 0.67	61.67 $\pm$ 0.88	59.33 $\pm$ 0.69	<b>66.67<math>\pm</math>0.58</b>	67.67 $\pm$ 0.19	70.33 $\pm$ 0.38	67.00 $\pm$ 0.51	<b>75.00<math>\pm</math>0.67</b>
Math Reasoning	WeMath	5.8k	31.49 $\pm$ 0.15	35.00 $\pm$ 0.17	35.92 $\pm$ 0.18	<b>36.84<math>\pm</math>0.13</b>	58.33 $\pm$ 0.10	62.87 $\pm$ 0.11	57.30 $\pm$ 0.09	<b>63.97<math>\pm</math>0.09</b>	58.47 $\pm$ 0.00	68.10 $\pm$ 0.03	59.19 $\pm$ 0.13	<b>70.75<math>\pm</math>0.07</b>
	MathVision	2.8k	17.04 $\pm$ 0.09	16.74 $\pm$ 0.00	16.89 $\pm$ 0.40	<b>17.04<math>\pm</math>0.38</b>	23.62 $\pm$ 0.31	23.77 $\pm$ 0.30	22.42 $\pm$ 0.23	<b>27.35<math>\pm</math>0.52</b>	27.20 $\pm$ 0.30	27.35 $\pm$ 0.43	23.92 $\pm$ 0.17	<b>30.19<math>\pm</math>0.26</b>
	DynaMath	4.0k	14.47 $\pm$ 0.00	26.65 $\pm$ 0.30	28.44 $\pm$ 0.06	<b>28.54<math>\pm</math>0.17</b>	36.92 $\pm$ 0.06	35.33 $\pm$ 0.25	36.72 $\pm$ 0.20	<b>38.52<math>\pm</math>0.06</b>	33.63 $\pm$ 0.17	36.23 $\pm$ 0.17	34.13 $\pm$ 0.23	<b>41.42<math>\pm</math>0.23</b>
OCR QA	OCRQA	801.6k	60.99 $\pm$ 0.01	65.96 $\pm$ 0.01	65.62 $\pm$ 0.01	<b>67.33<math>\pm</math>0.01</b>	79.73 $\pm$ 0.02	81.28 $\pm$ 0.00	72.98 $\pm$ 0.01	<b>81.46<math>\pm</math>0.02</b>	76.69 $\pm$ 0.01	81.02 $\pm$ 0.01	77.37 $\pm$ 0.02	<b>81.39<math>\pm</math>0.01</b>
	TextVQA	34.6k	47.80 $\pm$ 0.00	50.24 $\pm$ 0.05	50.00 $\pm$ 0.04	<b>50.56<math>\pm</math>0.04</b>	71.14 $\pm$ 0.04	73.30 $\pm$ 0.02	71.26 $\pm$ 0.02	<b>73.34<math>\pm</math>0.06</b>	72.20 $\pm$ 0.01	72.94 $\pm$ 0.05	71.52 $\pm$ 0.05	<b>73.28<math>\pm</math>0.02</b>
	ST-VQA	20.9k	52.16 $\pm$ 0.03	54.99 $\pm$ 0.05	54.59 $\pm$ 0.05	<b>55.74<math>\pm</math>0.04</b>	82.03 $\pm$ 0.06	84.23 $\pm$ 0.04	80.86 $\pm$ 0.03	<b>84.37<math>\pm</math>0.04</b>	81.27 $\pm$ 0.04	82.72 $\pm$ 0.01	80.19 $\pm$ 0.02	<b>82.86<math>\pm</math>0.02</b>
Structured QA	DocVQA	39.5k	21.82 $\pm$ 0.05	24.45 $\pm$ 0.04	23.70 $\pm$ 0.04	<b>25.37<math>\pm</math>0.04</b>	78.24 $\pm$ 0.02	91.64 $\pm$ 0.04	90.30 $\pm$ 0.06	<b>91.83<math>\pm</math>0.01</b>	92.67 $\pm$ 0.05	92.54 $\pm$ 0.04	92.05 $\pm$ 0.01	<b>92.88<math>\pm</math>0.05</b>
	ChartQA	28.3k	14.36 $\pm$ 0.12	19.00 $\pm$ 0.12	18.12 $\pm$ 0.07	<b>20.28<math>\pm</math>0.12</b>	71.84 $\pm$ 0.00	80.72 $\pm$ 0.02	71.76 $\pm$ 0.12	<b>80.84<math>\pm</math>0.08</b>	79.04 $\pm$ 0.02	79.88 $\pm$ 0.08	77.88 $\pm$ 0.09	<b>80.24<math>\pm</math>0.07</b>
GUI Grounding	RICO-ScreenQA	69.0k	32.23 $\pm$ 0.02	41.59 $\pm$ 0.03	39.92 $\pm$ 0.02	<b>42.93<math>\pm</math>0.01</b>	82.01 $\pm$ 0.01	86.18 $\pm$ 0.01	80.43 $\pm$ 0.02	<b>87.31<math>\pm</math>0.03</b>	82.18 $\pm$ 0.03	89.36 $\pm$ 0.01	81.01 $\pm$ 0.02	<b>89.59<math>\pm</math>0.03</b>
Domain-Specific	RSVQA	16.1k	50.90 $\pm$ 0.26	89.10 $\pm$ 0.32	88.40 $\pm$ 0.23	<b>89.90<math>\pm</math>0.31</b>	62.30 $\pm$ 0.29	87.70 $\pm$ 0.06	63.50 $\pm$ 0.26	<b>87.90<math>\pm</math>0.26</b>	61.00 $\pm$ 0.23	86.80 $\pm$ 0.25	58.90 $\pm$ 0.23	<b>88.30<math>\pm</math>0.26</b>
	VQA-RAD	1.8k	37.25 $\pm$ 0.26	51.22 $\pm$ 0.59	50.11 $\pm$ 0.34	<b>51.66<math>\pm</math>0.59</b>	59.87 $\pm$ 0.13	62.75 $\pm$ 0.22	59.42 $\pm$ 0.26	<b>63.64<math>\pm</math>0.22</b>	57.64 $\pm$ 0.46	59.42 $\pm$ 0.26	56.32 $\pm$ 0.64	<b>62.30<math>\pm</math>0.38</b>

**Table 3: Ablation on the WeMath benchmark with LLaVA-1.5-7B and Qwen3-VL-8B. We evaluate all combinations of MaLoRA:  $\mathcal{L}_{\text{mmd}}$ ,  $\mathcal{L}_{\text{gram}}$ , and  $\mathcal{L}_{\text{gate}}$ .**

Components			Model	
$\mathcal{L}_{\text{mmd}}$	$\mathcal{L}_{\text{gram}}$	$\mathcal{L}_{\text{gate}}$	LLaVA-1.5-7B	Qwen3-VL-8B
			35.00 $\pm$ 0.11	68.10 $\pm$ 0.13
		✓	36.78 $\pm$ 0.03 $\uparrow$ 1.78	69.88 $\pm$ 0.17 $\uparrow$ 1.78
	✓		36.15 $\pm$ 0.15 $\uparrow$ 1.15	68.74 $\pm$ 0.11 $\uparrow$ 0.64
✓			36.67 $\pm$ 0.13 $\uparrow$ 1.67	68.16 $\pm$ 0.17 $\uparrow$ 0.06
	✓	✓	36.67 $\pm$ 0.11 $\uparrow$ 1.67	69.66 $\pm$ 0.06 $\uparrow$ 1.56
✓		✓	36.61 $\pm$ 0.15 $\uparrow$ 1.61	70.00 $\pm$ 0.13 $\uparrow$ 1.90
✓	✓		36.32 $\pm$ 0.07 $\uparrow$ 1.32	68.62 $\pm$ 0.06 $\uparrow$ 0.52
✓	✓	✓	<b>36.84<math>\pm</math>0.17<math>\uparrow</math>1.84</b>	<b>70.75<math>\pm</math>0.14<math>\uparrow</math>2.65</b>

on the two Qwen backbones, where MaLoRA ranks first on every benchmark. On LLaVA-1.5-7B, it also improves over LoRA on nearly all tasks and never drops below the best competing setting. The largest gains appear on visually demanding benchmarks such as DynaMath, MMStar, MathVision, ChartQA, and MMBench-EN, suggesting that the method is particularly effective when success depends on reliable use of image evidence rather than text priors.

To better understand this behavior, Figure 3 shows a representative failure example from VQAv2 subsets [6]. In this example, the base model and LoRA are distracted by misleading text and fail to use the critical visual cues. MaLoRA instead grounds the prediction in the image and produces the correct answer. Additional quantitative analysis is provided in the appendix.

*Stronger gains on vision-critical tasks.* The gains from MaLoRA are most pronounced on tasks where visual evidence is essential. The clearest improvements appear in math-heavy benchmarks, with

the largest single gain observed on **DynaMath** for Qwen3-VL-8B. Similar trends also appear on other visually intensive benchmarks, including **MathVision**, **MMStar**, and **ChartQA**. By contrast, tasks that are less sensitive to cross-modal mismatch tend to show smaller but still consistent improvements. Overall, this pattern suggests that MaLoRA is most helpful when the model must resolve fine-grained visual structure, such as diagrams, charts, layouts, or spatial cues, rather than relying on language shortcuts.

### 5.3 Ablation Study

To isolate the contribution of each component in MaLoRA, we conduct a full combinatorial ablation on the WeMath benchmark using **LLaVA-1.5-7B** and **Qwen3-VL-8B** (Table 3). Every MaLoRA variant improves over standard LoRA, and the full model consistently performs best on both backbones, confirming that the three objectives are complementary rather than redundant.

Among single-component variants, all three objectives yield consistent gains over the LoRA baseline. Combining  $\mathcal{L}_{\text{gate}}$  with either  $\mathcal{L}_{\text{mmd}}$  or  $\mathcal{L}_{\text{gram}}$  further improves results, whereas using  $\mathcal{L}_{\text{mmd}}$  and  $\mathcal{L}_{\text{gram}}$  without  $\mathcal{L}_{\text{gate}}$  is less effective, especially on Qwen3-VL-8B. The best performance is achieved when all three objectives are active, suggesting that reducing cross-modal discrepancy is most effective when paired with modality-aware adaptation and structural preservation in the key space.

Since the gated dual-branch architecture itself introduces additional modality-specific capacity compared to standard LoRA, a natural question is whether the observed gains stem from the alignment objectives or simply from increased expressiveness. To disentangle these two factors, we provide a parameter-matched control experiment in Appendix, along with a hyperparameter sensitivity analysis for the three loss terms.

### 5.4 Cross-modal Key-space Divergence

Our central hypothesis is that multimodal reasoning is hindered by a geometric mismatch between visual and textual representations in the projected key space. This space is particularly important

**Table 4: Cross-modal key distribution alignment at the early layer for LLaVA-1.5-7B, Qwen2.5-VL-7B, and Qwen3-VL-8B on MMBench-EN and MMMU. MMD and JS divergence quantify the representation gap between image and text features in the projected key space.**

MMD							JS						
Setting	LLaVA-1.5-7B		Qwen2.5-VL-7B		Qwen3-VL-8B		Setting	LLaVA-1.5-7B		Qwen2.5-VL-7B		Qwen3-VL-8B	
	MMB-EN	MMMU	MMB-EN	MMMU	MMB-EN	MMMU		MMB-EN	MMMU	MMB-EN	MMMU	MMB-EN	MMMU
Base	0.51	0.54	0.93	0.89	0.44	0.44	Base	0.54	0.45	0.89	0.86	0.47	0.50
Ours	0.44	0.51	0.82	0.71	0.41	0.41	Ours	0.37	0.40	0.79	0.82	0.40	0.35
$\Delta$	0.07	0.03	0.11	0.18	0.03	0.03	$\Delta$	0.17	0.05	0.10	0.04	0.07	0.15

because attention weights are determined by query–key similarity: if visual keys are systematically separated from textual states, then visual evidence becomes harder for textual queries to retrieve during decoding. To test this hypothesis, we measure the divergence between image and text representations in the projected key space using both MMD and Jensen–Shannon (JS) divergence.

Table 4 reports the results at the early layer for all three backbones on MMBench-EN and MMMU, while the corresponding middle- and late-layer results are provided in Appendix Table 11. Across all backbones and datasets, the base models consistently exhibit a clear gap between visual and textual key distributions, indicating that cross-modal misalignment already appears at shallow layers rather than emerging only in deeper processing stages.

After applying MaLoRA, both divergence measures decrease consistently across all model–dataset pairs. At the early layer, MMD is reduced by 0.03–0.18 and JS by 0.04–0.17. These reductions show that MaLoRA directly acts on the hypothesized bottleneck by bringing visual and textual keys into a more compatible geometric configuration. The effect is especially strong for Qwen2.5-VL-7B, which exhibits the largest MMD decrease on both benchmarks, while LLaVA-1.5-7B and Qwen3-VL-8B also show stable improvements under both metrics.

Importantly, this pattern is not limited to shallow layers. As shown in Appendix Table 11, the reduction in cross-modal divergence persists through the middle and late layers. Taken together, these results support our hypothesis that key-space misalignment is a persistent property of current MLLMs and suggest that MaLoRA improves multimodal reasoning by alleviating this mismatch at its geometric source.

## 5.5 Cross-domain Transfer

To assess whether key-space alignment generalizes beyond the training distribution, we fine-tune each model on a single source domain (**WeMath**) and evaluate directly on nine out-of-domain benchmarks without further adaptation (Table 5).

On **Qwen2.5-VL-7B**, MaLoRA outperforms LoRA on all nine benchmarks, improving OCR-VQA (82.29 vs. 80.66), ChartQA (78.28 vs. 78.16), DocVQA (90.26 vs. 89.77), SimpleVQA (39.55 vs. 38.20), TextVQA (72.58 vs. 71.66), Remote (60.80 vs. 60.70), ST-VQA (81.69 vs. 80.79), DynaMath (33.13 vs. 32.93), and MathVision (22.57 vs. 21.08). In several cases where LoRA falls substantially below the Base checkpoint, MaLoRA consistently recovers part of the performance.

For **LLaVA-1.5-7B**, MaLoRA also reduces cross-domain degradation and outperforms LoRA on all reported benchmarks, with

especially large gains on **RAD** (44.57 vs. 37.92), **ST-VQA** (50.58 vs. 45.98), and **Remote** (52.90 vs. 51.40). Although the Base checkpoint remains strongest on some general-domain tasks, MaLoRA preserves more transferable capability than LoRA after single-domain fine-tuning. These results suggest that reducing the key-space gap during adaptation improves robustness under distribution shift.

## 5.6 Attention Redistribution

If the reduction in key-space divergence is functionally meaningful, it should also influence attention allocation by making visual tokens more accessible to textual queries. We therefore examine the layer-wise relative change in aggregated Text  $\rightarrow$  Visual attention compared to the corresponding base model.

As shown in Figure 4, MaLoRA increases Text  $\rightarrow$  Visual attention in most layers of LLaVA-1.5-7B on both MMMU and MMBench, suggesting improved access to visual evidence during decoding. The increase is most pronounced in the early layers, where cross-modal interactions are first formed. Results for Qwen2.5-VL-7B and Qwen3-VL-8B, provided in the appendix, show a similar pattern.

Together with the divergence analysis above, these results support the proposed mechanism: reducing the geometric mismatch between visual and textual keys leads to greater attention from text tokens to visual evidence during reasoning.

## 5.7 Training and Inference Cost

Table 6 compares MaLoRA, LoRA, and QLoRA on **Qwen2.5-VL-7B** under the same hardware and batch settings. Compared with LoRA, MaLoRA increases peak GPU memory only slightly from **18.85 GB** to **19.24 GB** (+2.1%) and per-step time from **199.66 s** to **221.41 s** (+10.9%). Its trainable parameters account for **2.80%** of the base model, only marginally higher than LoRA’s **2.49%**.

At inference, LoRA adds almost no overhead after weight merging (+0.64%), whereas MaLoRA incurs a +30.75% latency overhead due to per-token gating in each  $k_{\text{proj}}$  layer. However, this figure is measured with only **20 output tokens**, where the one-time prefill cost dominates. During autoregressive decoding, each step passes only a single token through a lightweight sigmoid MLP, whose  $O(d)$  cost is negligible relative to attention  $O(d \times L)$  and FFN  $O(d \times d_{\text{ff}})$ , so the relative overhead diminishes as generation length grows. QLoRA shows the highest latency (+216.80%) due to repeated dequantization. Overall, MaLoRA offers a practical trade-off: modest training overhead, strong accuracy gains.

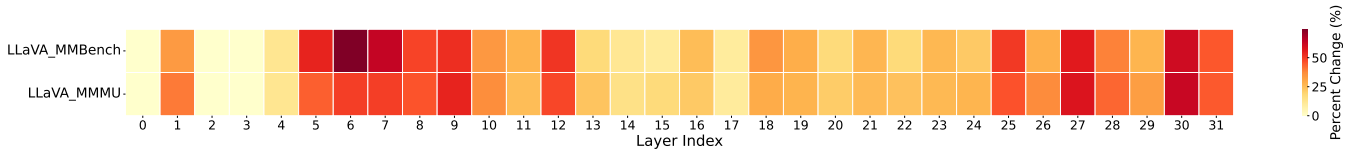


**Figure 4: Layer-wise relative change (%) in aggregated Text→Visual attention after MaLoRA fine-tuning, measured with respect to the corresponding base model across LLaVA-1.5-7B on MMMU and MMBench. Positive values indicate that textual queries allocate a larger proportion of attention to visual keys after fine-tuning.**

**Table 5: Cross-domain transfer results. We fine-tune on WeMath2 datasets and evaluate directly on target benchmarks without further adaptation. Base uses the original instruct checkpoint with no fine-tuning. Bold indicates the best among all methods; underline indicates Ours outperforms LoRA but does not surpass Base.**

Qwen2.5-VL-7B (fine-tuned on WeMath2)										
Method	OCRVQA	ChartQA	DocVQA	SimpleVQA	TextVQA	Remote	ST-VQA	DynaMath	MathVision	MMBench-EN
Base	79.73	71.84	78.24	35.51	71.14	62.30	82.03	36.92	23.62	90.30
LoRA	80.66	78.16	89.77	38.20	71.66	60.70	80.79	32.93	21.08	88.68
QLoRA	32.75	17.44	67.53	18.20	44.28	34.80	48.26	22.06	7.03	88.91
Ours	<b>82.29</b>	<b>78.28</b>	<b>90.26</b>	<b>39.55</b>	<b>72.58</b>	<u>60.80</u>	<u>81.69</u>	<u>33.13</u>	<u>22.57</u>	<u>88.91</u>
LLaVa-1.5-7B (fine-tuned on WeMath2)										
Method	OCRVQA	ChartQA	DocVQA	SimpleVQA	TextVQA	Remote	ST-VQA	DynaMath	MathVision	MMBench-EN
Base	60.99	14.36	21.82	14.16	47.80	50.90	52.16	14.47	17.04	72.52
LoRA	58.26	13.08	20.79	14.61	46.50	51.40	45.98	15.46	12.26	71.36
QLoRA	58.68	13.04	19.99	17.53	45.98	51.80	50.76	24.55	12.11	71.36
Ours	<u>58.80</u>	<u>13.32</u>	<u>20.85</u>	<b>14.83</b>	<u>46.74</u>	<b>52.90</b>	<u>50.58</u>	<b>15.57</b>	<u>12.86</u>	<u>72.17</u>

**Table 6: Training and inference cost on Qwen2.5-VL-7B. Peak GPU Mem (GB) denotes maximum training memory, Step Time (s) the average time per optimization step, Params Added the number of trainable parameters, and Inference Overhead the per-sample latency relative to Base, measured over 5 GPU runs with 20 output tokens.**

Method	Peak GPU Mem (GB)	Step Time (s)	Params Added	Inference Overhead
Base	16.87	237.26	0.00%	+0.00%
LoRA	18.85	199.66	2.49%	+0.64%
QLoRA	9.24	474.86	2.49%	+216.80%
Ours	19.24	221.41	2.80%	+30.75%

## 5.8 Scaling Behavior

We further evaluate MaLoRA across four model scales of Qwen2.5-VL (3B, 7B, 32B, and 72B) on MMStar (Table 7). MaLoRA consistently outperforms both Base and LoRA at every scale, achieving **58.67** vs. **57.33** (LoRA) at 3B, **66.67** vs. **61.67** at 7B, **71.67** vs. **70.00** at 32B, and **73.67** vs. **71.33** at 72B. The absolute gain over LoRA ranges from **+1.34** to **+5.00**, with the largest improvement at 7B. Notably, at 7B, LoRA even underperforms the Base checkpoint (61.67 vs. 65.67), whereas MaLoRA surpasses both. These results indicate that the benefit of key-space alignment scales well with model capacity and remains effective from small to large multimodal backbones.

**Table 7: Comparison of the Base model (without task-specific fine-tuning), LoRA, and our method on MMStar across different sizes of the Qwen2.5-VL model family.**

Method	Qwen2.5-VL-3B	Qwen2.5-VL-7B	Qwen2.5-VL-32B	Qwen2.5-VL-72B
Base	55.67	65.67	65.00	65.33
LoRA	57.33	61.67	70.00	71.33
Ours	<b>58.67</b>	<b>66.67</b>	<b>71.67</b>	<b>73.67</b>

## 6 Conclusion

In this paper, we show that cross-modal misalignment in the attention key space is an important source of text-centric bias in multimodal large language models. To mitigate this issue, we propose MaLoRA, a parameter-efficient fine-tuning framework that combines modality-specific key adaptation, cross-modal distribution alignment, and structure-preserving regularization. Experiments on multiple MLLM backbones and benchmarks show that MaLoRA consistently reduces the gap between visual and textual key representations and improves downstream performance, particularly on tasks that depend heavily on visual evidence. Overall, these findings suggest that aligning the attention key space is a simple and effective way to reduce modality bias in multimodal fine-tuning.

## Acknowledgments

To Robert, for the bagels and explaining CMYK and color spaces.

## References

- [1] Ali Furkan Biten, Ruben Tito, Andres Mafra, Lluís Gomez, Marçal Rusinol, Ernest Valveny, CV Jawahar, and Dimosthenis Karatzas. 2019. Scene text visual question answering. In *Proceedings of the IEEE/CVF international conference on computer vision*. 4291–4301.
- [2] Lin Chen, Jinsong Li, Xiaoyi Dong, Pan Zhang, Conghui He, Jiaqi Wang, Feng Zhao, and Dahua Lin. 2024. Sharegpt4v: Improving large multi-modal models with better captions. In *European Conference on Computer Vision*. Springer, 370–387.
- [3] Lin Chen, Jinsong Li, Xiaoyi Dong, Pan Zhang, Yuhang Zang, Zehui Chen, Haodong Duan, Jiaqi Wang, Yu Qiao, Dahua Lin, et al. 2024. Are we on the right way for evaluating large vision-language models? *Advances in Neural Information Processing Systems* 37 (2024), 27056–27087.
- [4] Xiwen Chen, Wenhui Zhu, Peijie Qiu, Hao Wang, Huayu Li, Haiyu Wu, Aristeidis Sotiras, Yalin Wang, and Abolfazl Razi. 2025. Prompt-OT: An Optimal Transport Regularization Paradigm for Knowledge Preservation in Vision-Language Model Adaptation. *arXiv preprint arXiv:2503.08906* (2025).
- [5] Xianfu Cheng, Wei Zhang, Shiwei Zhang, Jian Yang, Xiangyuan Guan, Xianjie Wu, Xiang Li, Ge Zhang, Jiaheng Liu, Yuying Mai, et al. 2025. Simplevqa: Multimodal factuality evaluation for multimodal large language models. In *Proceedings of the IEEE/CVF International Conference on Computer Vision*. 4637–4646.
- [6] Ailin Deng, Tri Cao, Zhirui Chen, and Bryan Hooi. 2025. Words or vision: Do vision-language models have blind faith in text?. In *Proceedings of the Computer Vision and Pattern Recognition Conference*. 3867–3876.
- [7] Arthur Gretton, Karsten M Borgwardt, Malte J Rasch, Bernhard Schölkopf, and Alexander Smola. 2012. A kernel two-sample test. *The journal of machine learning research* 13, 1 (2012), 723–773.
- [8] Yu-Chung Hsiao, Fedir Zubach, Gilles Baechler, Srinivas Sunkara, Victor Cărbune, Jason Lin, Maria Wang, Yun Zhu, and Jindong Chen. 2025. Screenqa: Large-scale question-answer pairs over mobile app screenshots. In *Proceedings of the 2025 Conference of the Nations of the Americas Chapter of the Association for Computational Linguistics: Human Language Technologies (Volume 1: Long Papers)*. 9427–9452.
- [9] Qidong Huang, Xiaoyi Dong, Pan Zhang, Bin Wang, Conghui He, Jiaqi Wang, Dahua Lin, Weiming Zhang, and Nenghai Yu. 2024. Opera: Alleviating hallucination in multi-modal large language models via over-trust penalty and retrospection-allocation. In *Proceedings of the IEEE/CVF Conference on Computer Vision and Pattern Recognition*. 13418–13427.
- [10] Zhehan Kan, Ce Zhang, Zihan Liao, Yapeng Tian, Wenming Yang, Junyuan Xiao, Xu Li, Dongmei Jiang, Yaowei Wang, and Qingmin Liao. 2024. Catch: Complementary adaptive token-level contrastive decoding to mitigate hallucinations in llms. *arXiv preprint arXiv:2411.12713* (2024).
- [11] Jason J Lau, Soumya Gayen, Asma Ben Abacha, and Dina Demner-Fushman. 2018. A dataset of clinically generated visual questions and answers about radiology images. *Scientific data* 5, 1 (2018), 180251.
- [12] Sicong Leng, Hang Zhang, Guanzheng Chen, Xin Li, Shijian Lu, Chunyan Miao, and Lidong Bing. 2024. Mitigating object hallucinations in large vision-language models through visual contrastive decoding. In *Proceedings of the IEEE/CVF Conference on Computer Vision and Pattern Recognition*. 13872–13882.
- [13] Chenxi Liu, Tianyi Xiong, Yanshuo Chen, Ruibo Chen, Yihan Wu, Junfeng Guo, Tianyi Zhou, and Heng Huang. 2025. Modality-balancing preference optimization of large multimodal models by adversarial negative mining. *arXiv preprint arXiv:2506.08022* (2025).
- [14] Yuan Liu, Haodong Duan, Yuanhan Zhang, Bo Li, Songyang Zhang, Wangbo Zhao, Yike Yuan, Jiaqi Wang, Conghui He, Ziwei Liu, et al. 2024. Mmbench: Is your multi-modal model an all-around player?. In *European conference on computer vision*. Springer, 216–233.
- [15] Sylvain Lobry, Diego Marcos, Jesse Murray, and Devis Tuia. 2020. RSVQA: Visual question answering for remote sensing data. *IEEE Transactions on Geoscience and Remote Sensing* 58, 12 (2020), 8555–8566.
- [16] Ahmed Masry, Xuan Long Do, Jia Qing Tan, Shafiq Joty, and Enamul Hoque. 2022. Chartqa: A benchmark for question answering about charts with visual and logical reasoning. In *Findings of the association for computational linguistics: ACL 2022*. 2263–2279.
- [17] Minesh Mathew, Dimosthenis Karatzas, and CV Jawahar. 2021. Docvqa: A dataset for vqa on document images. In *Proceedings of the IEEE/CVF winter conference on applications of computer vision*. 2200–2209.
- [18] Anand Mishra, Shashank Shekhar, Ajeet Kumar Singh, and Anirban Chakraborty. 2019. Ocr-vqa: Visual question answering by reading text in images. In *2019 international conference on document analysis and recognition (ICDAR)*. IEEE, 947–952.
- [19] Jean Park, Kuk Jin Jang, Basam Alasaly, Sriharsha Mopidevi, Andrew Zolensky, Eric Eaton, Insup Lee, and Kevin Johnson. 2025. Assessing modality bias in video question answering benchmarks with multimodal large language models. In *Proceedings of the AAAI Conference on Artificial Intelligence*, Vol. 39. 19821–19829.
- [20] Runqi Qiao, Qiuna Tan, Guanting Dong, MinhuiWu MinhuiWu, Chong Sun, Xiaoshuai Song, Jiapeng Wang, Zhuoma Gongque, Shanglin Lei, Yifan Zhang, et al. 2025. We-math: Does your large multimodal model achieve human-like mathematical reasoning?. In *Proceedings of the 63rd Annual Meeting of the Association for Computational Linguistics (Volume 1: Long Papers)*. 20023–20070.
- [21] Amanpreet Singh, Vivek Natarajan, Meet Shah, Yu Jiang, Xinlei Chen, Dhruv Batra, Devi Parikh, and Marcus Rohrbach. 2019. Towards vqa models that can read. In *Proceedings of the IEEE/CVF conference on computer vision and pattern recognition*. 8317–8326.
- [22] Zijia Song, Zelin Zang, Yelin Wang, Guozheng Yang, Wanyu Chen, Miaoyu Wang, Stan Z Li, et al. 2024. Set-clip: Exploring aligned semantic from low-alignment multimodal data through a distribution view. *arXiv preprint arXiv:2406.05766* (2024).
- [23] Jingchen Sun, Rohan Sharma, Vishnu Suresh Lokhande, and Changyou Chen. 2024. Craft: Cross-modal Aligned Features Improve Robustness of Prompt Tuning. *arXiv preprint arXiv:2407.15894* (2024).
- [24] Zhiqing Sun, Sheng Shen, Shengcao Cao, Haotian Liu, Chunyuan Li, Yikang Shen, Chuang Gan, Liangyan Gui, Yu-Xiong Wang, Yiming Yang, et al. 2024. Aligning large multimodal models with factually augmented rlhf. In *Findings of the Association for Computational Linguistics: ACL 2024*. 13088–13110.
- [25] Ke Wang, Juntong Pan, Weikang Shi, Zimu Lu, Houxing Ren, Aojun Zhou, Mingjie Zhan, and Hongsheng Li. 2024. Measuring multimodal mathematical reasoning with math-vision dataset. *Advances in Neural Information Processing Systems* 37 (2024), 95095–95169.
- [26] Xintong Wang, Jingheng Pan, Liang Ding, and Chris Biemann. 2024. Mitigating hallucinations in large vision-language models with instruction contrastive decoding. *arXiv preprint arXiv:2403.18715* (2024).
- [27] Huyu Wu, Meng Tang, Xinhan Zheng, and Haiyun Jiang. 2025. When Language Overrules: Revealing Text Dominance in Multimodal Large Language Models. *arXiv preprint arXiv:2508.10552* (2025).
- [28] Shukang Yin, Chaoyou Fu, Sirui Zhao, Tong Xu, Hao Wang, Dianbo Sui, Yunhang Shen, Ke Li, Xing Sun, and Enhong Chen. 2024. Woodpecker: Hallucination correction for multimodal large language models. *Science China Information Sciences* 67, 12 (2024), 220105.
- [29] Xiang Yue, Yuansheng Ni, Kai Zhang, Tianyu Zheng, Ruoqi Liu, Ge Zhang, Samuel Stevens, Dongfu Jiang, Weiming Ren, Yuxuan Sun, et al. 2024. Mmmu: A massive multi-discipline multimodal understanding and reasoning benchmark for expert agi. In *Proceedings of the IEEE/CVF conference on computer vision and pattern recognition*. 9556–9567.
- [30] Zexuan Zhao, Wen Wang, Qiang Long, Wenwang Zhu, Binxing Jiao, and Yu Lan. 2025. Looking Beyond Text: Reducing Language Bias in Large Vision-Language Models. In *Proceedings of the 2025 Conference on Empirical Methods in Natural Language Processing (EMNLP)*. <https://aclanthology.org/2025.emnlp-main.995/>

## A Settings

### A.1 Benchmarks and Experimental Settings

We evaluate three instruction-tuned models (LLaVA-1.5-7B, Qwen2.5-VL-7B, Qwen3-VL-8B) on public benchmarks across five core capability dimensions, covering general understanding, expert reasoning, math reasoning, Optical Character Recognition Question Answering (OCR QA), structured QA, GUI Grounding, and domain-specific tasks. The performance comparison includes four training setups (Base, LoRA, QLoRA, Ours). Detailed benchmarks used in this experiment are listed below:

**General Understanding:** One benchmark is selected to assess the models’ basic vision-language understanding capabilities, namely the English version of MMBench (MMBench-EN).

**Expert Reasoning:** Two benchmarks are chosen to cover basic visual factual QA and multimodal subjective star rating evaluation, including SimpleVQA (a multimodal factuality evaluation benchmark) and MMStar (a multimodal star rating evaluation benchmark).

**Math Reasoning:** Three benchmarks focusing on visual math reasoning are adopted, covering human-level visual math, static visual math scenarios, and dynamic visual math robustness evaluation, including WeMath (a human-level visual math reasoning benchmark), MathVision (a visual math reasoning dataset), and DynaMath (a dynamic visual math reasoning robustness benchmark).

**Optical Character Recognition Question Answering (OCR QA):** Three benchmarks are selected to evaluate OCR and text-visual QA capabilities, including OCRVQA (an OCR-based visual question answering benchmark), TextVQA (a text-based visual question answering benchmark), and ST-VQA (a scene text visual question answering benchmark).

**Structured QA:** Two benchmarks targeting structured understanding of documents and charts are selected, including DocVQA (a document image visual question answering benchmark) and ChartQA (a chart question answering reasoning benchmark).

**GUI Grounding:** One benchmark for evaluating GUI element localization capabilities is used, namely RICO-ScreenQA (a RICO screen visual question answering benchmark).

**Domain-Specific:** Two vertical domain benchmarks are chosen to cover remote sensing and medical image understanding, including RSVQA (a remote sensing benchmark) and VQA-RAD (a medical image visual question answering benchmark).

Table 8 systematically lists the core configurations and general optimization training parameters for LoRA fine-tuning in this study. The upper section clarifies LoRA-specific hyperparameters such as rank, scaling factor, dropout probability, and target training modules, while the lower section standardizes unified training process configurations including global batch size, learning rate schedule, and precision settings. This provides a reproducible benchmark framework for LoRA and QLoRA fine-tuning of all models.

LoRA Fine-tuning Settings	
Parameter	Value
LoRA rank ( $r$ )	16
LoRA scaling ( $\alpha$ )	32
LoRA dropout	0.05
Target modules	q_proj, k_proj, v_proj, o_proj
Bias	none
Trainable params	LoRA only
Optimization & Training	
Global batch size	256
Micro batch size	1
Gradient accumulation	256
Learning rate	2e-4
LR scheduler	cosine
Warmup steps	100
Weight decay	0.0
Max grad norm	1.0
Precision	bf16
Max seq length	4096
Num epochs	1

**Table 8: Hyperparameter configuration for LoRA fine-tuning. The table is divided into two sections: LoRA-specific settings and general optimization/training settings.**

### A.2 Data Sources and Split Statistics

To ensure transparency and reproducibility of our experimental setup, we provide dataset source descriptions, split strategies, and sample-size statistics in this section. In general, for datasets with official train/test (or train/validation/test) protocols, we strictly follow the official splits;

for datasets without official splits, we randomly partition all available samples into training and test sets with an 8:2 ratio, using a fixed random seed for reproducibility.

For example, OCR-VQA follows the official train/validation/test split; MMBench-EN follows the official dev/test split; and VQA-RAD follows the official train/test split. For datasets without official split definitions, we construct training and test sets according to the same 8:2 rule.

### A.3 Grid Search Experimental Details

To systematically explore the hyperparameter space of the three loss terms in our method, we conducted a comprehensive grid search experiment on Dataset MMStar using the Qwen3-VL-8B model. The search space covers three loss weights:  $\lambda_{\text{mmd}}$  (MMD loss coefficient),  $\lambda_{\text{gram}}$  (Gram matrix reference loss coefficient), and  $\lambda_{\text{gate}}$  (gate supervision loss coefficient).

**Search Space Design.** We adopt a  $3 \times 3 \times 3$  full factorial design, resulting in 27 unique experimental configurations. The specific search ranges are:

- $\lambda_{\text{mmd}} \in \{0.05, 0.15, 0.3\}$
- $\lambda_{\text{gram}} \in \{0.01, 0.05, 0.1\}$
- $\lambda_{\text{gate}} \in \{0.05, 0.1, 0.15\}$

All experiments were completed successfully, with a total computational cost of approximately 4.5 hours (average 10.0 minutes per experiment). Table 9 presents the complete experimental configurations in a compact factorial layout, where each cell corresponds to a specific hyperparameter combination.

**Table 9: Grid Search:  $3 \times 3 \times 3$  Factorial Design. Cell values are experiment IDs.**

$\lambda_{\text{mmd}} \setminus \lambda_{\text{gram}}$	$\lambda_{\text{gate}} = 0.05$			$\lambda_{\text{gate}} = 0.10$			$\lambda_{\text{gate}} = 0.15$		
	0.01	0.05	0.10	0.01	0.05	0.10	0.01	0.05	0.10
0.05	01	04	07	02	05	08	03	06	09
0.15	10	13	16	11	14	17	12	15	18
0.30	19	22	25	20	23	26	21	24	27

For reproducibility, Table 10 provides the complete experimental metadata including experiment IDs, exact hyperparameter values, duration and evaluation scores.

The grid search results enable us to analyze the individual and interaction effects of different loss terms on model performance. Based on these experiments, we select the optimal hyperparameter configuration for subsequent evaluations on the full benchmark suite.

## B Additional Analysis and Experimental Results

### B.1 Cross-modal Key-space Divergence at Middle and Late Layers

Table 11 complements the early-layer analysis in the main text by reporting the divergence between visual and textual key distributions at the middle and late layers. Consistent with the main-text results, MaLoRA reduces cross-modal discrepancy under both MMD and Jensen–Shannon (JS) divergence across most model–dataset pairs on MMBench-EN and MMMU for all three backbones. At the middle layer, the reduction remains clearly visible, indicating that the improvement in visual–textual alignment is preserved beyond shallow representations after several layers of multimodal interaction. A similar trend is also observed at the late layer: although the absolute divergence values and the magnitude of improvement vary more across settings, MaLoRA still lowers cross-modal divergence in most cases. Overall, these results are consistent with the early-layer findings and suggest that the benefit of MaLoRA is not restricted to a single layer, but remains observable across different stages of the network.

### B.2 Image-Text Irrelevant Experiments

Beyond these general benchmarks, we also construct and use an image-text irrelevant test suite to evaluate model robustness under text-visual conflict conditions (i.e., when distracting text is irrelevant to visual evidence). Specifically, we adopt the image-text irrelevant subsets from Deng et al. [6] study as test data, and unify them into the test processed format, including three subsets: `vqav2_irrelevant`, `docvqa_irrelevant`, and `openphish_irrelevant`, with evaluation sizes of 1,000, 1,000, and 5,000, respectively. The corresponding results are reported in Table 12.

From Table 12, MaLoRA achieves the best performance across most settings, with the clearest gains on `openphish_irrelevant` (e.g., 5.24 vs. 2.48/2.04 for Qwen2.5-VL-7B, and 3.04 vs. 1.88/0.40 for Qwen3-VL-8B), indicating stronger robustness under severe irrelevant-text interference. On `vqav2_irrelevant` and `docvqa_irrelevant`, improvements are smaller but still consistent, suggesting that our method improves robustness while preserving strong baseline capability on relatively easier irrelevant scenarios.

As shown in Figure 5, we present two representative case studies under the irrelevant setting, where irrelevant textual distractors are inserted into the input and the model is expected to answer based on visual evidence. The results indicate that both the base Qwen3-VL-8B

**Table 10: Grid Search Hyperparameter Configurations for Loss Weight Tuning ( $3 \times 3 \times 3$  Factorial Design) with MMStar Evaluation Results**

Exp ID	$\lambda_{\text{mmd}}$	$\lambda_{\text{gram}}$	$\lambda_{\text{gate}}$	Train (min)	MMStar
01	0.05	0.01	0.05	7.5	73.67%
02	0.05	0.01	0.10	11.0	73.00%
03	0.05	0.01	0.15	11.9	72.00%
04	0.05	0.05	0.05	11.2	72.33%
05	0.05	0.05	0.10	11.4	72.00%
06	0.05	0.05	0.15	9.5	72.67%
07	0.05	0.10	0.05	9.7	73.33%
08	0.05	0.10	0.10	9.6	73.00%
09	0.05	0.10	0.15	9.3	72.00%
10	0.15	0.01	0.05	9.7	73.00%
11	0.15	0.01	0.10	7.9	74.67%
12	0.15	0.01	0.15	8.9	72.33%
13	0.15	0.05	0.05	8.7	73.00%
14	0.15	0.05	0.10	8.3	73.33%
15	0.15	0.05	0.15	9.1	72.33%
16	0.15	0.10	0.05	8.8	72.67%
17	0.15	0.10	0.10	10.2	72.00%
18	0.15	0.10	0.15	10.2	74.00%
19	0.30	0.01	0.05	12.3	71.67%
20	0.30	0.01	0.10	10.3	73.67%
21	0.30	0.01	0.15	10.3	73.67%
22	0.30	0.05	0.05	11.0	73.00%
23	0.30	0.05	0.10	10.4	73.67%
24	0.30	0.05	0.15	10.2	73.33%
25	0.30	0.10	0.05	10.1	73.00%
26	0.30	0.10	0.10	11.2	72.67%
27	0.30	0.10	0.15	11.1	75.00%

**Table 11: Cross-modal key distribution alignment at the middle and late layers for LLaVA-1.5-7B, Qwen2.5-VL-7B, and Qwen3-VL-8B on MMBench-EN and MMMU. MMD and JS divergence quantify the representation gap between image and text features in the projected key space. These additional results show that the alignment improvements of our method persist beyond shallow layers and remain observable at deeper network stages.****(a) Middle layer**

MMD							JS						
Setting	LLaVA-1.5-7B		Qwen2.5-VL-7B		Qwen3-VL-8B		Setting	LLaVA-1.5-7B		Qwen2.5-VL-7B		Qwen3-VL-8B	
	MMB-EN	MMMU	MMB-EN	MMMU	MMB-EN	MMMU		MMB-EN	MMMU	MMB-EN	MMMU	MMB-EN	MMMU
Base	0.43	0.43	0.06	0.06	0.12	0.11	Base	0.44	0.43	0.36	0.24	0.29	0.29
Ours	0.29	0.33	0.05	0.05	0.11	0.10	Ours	0.28	0.34	0.20	0.19	0.19	0.17
$\Delta$	0.14	0.10	0.01	0.01	0.01	0.01	$\Delta$	0.16	0.09	0.16	0.05	0.10	0.12

**(b) Late layer**

MMD							JS						
Setting	LLaVA-1.5-7B		Qwen2.5-VL-7B		Qwen3-VL-8B		Setting	LLaVA-1.5-7B		Qwen2.5-VL-7B		Qwen3-VL-8B	
	MMB-EN	MMMU	MMB-EN	MMMU	MMB-EN	MMMU		MMB-EN	MMMU	MMB-EN	MMMU	MMB-EN	MMMU
Base	0.16	0.22	0.04	0.23	0.02	0.02	Base	0.39	0.39	0.31	0.27	0.47	0.35
Ours	0.07	0.07	0.03	0.21	0.01	0.01	Ours	0.32	0.36	0.28	0.16	0.41	0.31
$\Delta$	0.09	0.15	0.01	0.02	0.01	0.01	$\Delta$	0.07	0.03	0.03	0.09	0.06	0.04

model and the LoRA-finetuned variant are more easily biased by textual priors, leading to errors such as incorrect counting and semantic misinterpretation of traffic signs. In contrast, the MaLoRA-finetuned model consistently ignores irrelevant text, focuses on key visual

Datasets	Qwen2.5-VL-7B				Qwen3-VL-8B			
	Base	LoRA	QLoRA	MaLoRA	Base	LoRA	QLoRA	MaLoRA
vqav2_irrelevant	68.4	71	58	71.8	70.7	71.8	66.9	72.2
openphish_irrelevant	1.6	2.48	2.04	5.24	0.91	1.88	0.4	3.04
docvqa_irrelevant	91.6	91.2	83.3	91.9	92.8	92.6	91.5	93.5

**Table 12: Performance (%) on the irrelevant benchmark subsets (vqav2\_irrelevant, openphish\_irrelevant, and docvqa\_irrelevant) for Qwen2.5-VL-7B and Qwen3-VL-8B under four fine-tuning settings: Base, LoRA, QLoRA, and MaLoRA.**

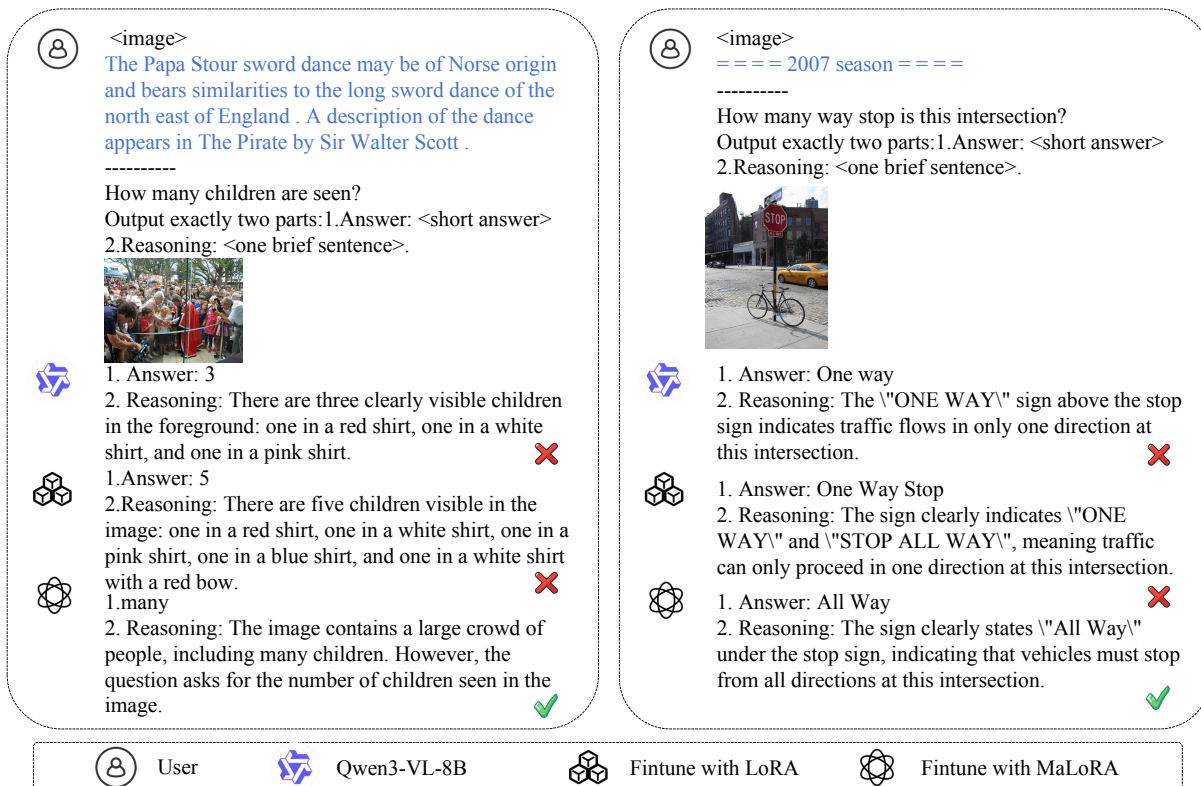


**Figure 5: Case studies on the irrelevant setting. When irrelevant textual distractors are added to the prompt, the base Qwen3-VL-8B and LoRA-finetuned models are more likely to be misled, while the MaLoRA-finetuned model remains grounded in visual evidence and produces correct answers.**

cues, and produces correct answers. These qualitative examples demonstrate that our method achieves stronger robustness and better vision-grounded alignment under text–vision conflict conditions.

### B.3 Modality Gap Metric

We use the modality gap metric to quantify the alignment between visual and textual representations in Figure 2. Here we provide the formal definition.

For a given transformer layer  $l$ , let  $\{\mathbf{v}_i\}_{i=1}^{N_v} \subset \mathbb{R}^d$  and  $\{\mathbf{t}_j\}_{j=1}^{N_t} \subset \mathbb{R}^d$  denote the key vectors extracted from visual tokens and text tokens, respectively. We first apply  $\ell_2$  normalization to each vector:

$$\hat{\mathbf{v}}_i = \frac{\mathbf{v}_i}{\|\mathbf{v}_i\|_2}, \quad \hat{\mathbf{t}}_j = \frac{\mathbf{t}_j}{\|\mathbf{t}_j\|_2}. \tag{8}$$

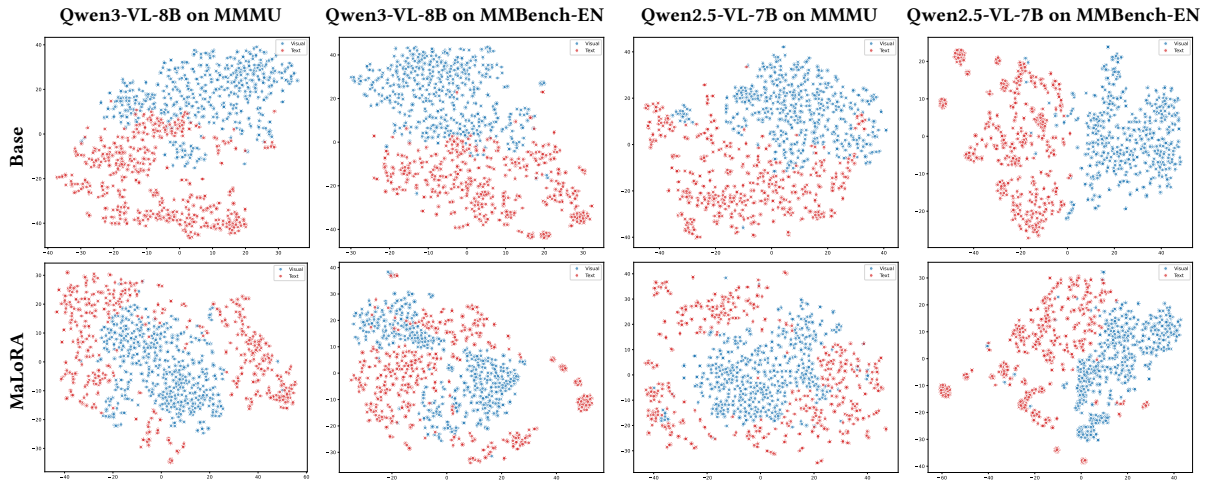


Figure 6: t-SNE visualization of hidden representations for Base and MaLoRA on Qwen3-VL-8B and Qwen2.5-VL-7B, evaluated on MMMU and MMBench-EN. Each column shows one model–dataset pair, and the two rows compare the Base model with MaLoRA.

The modality gap at layer  $l$  is then defined as the Euclidean distance between the centroids of the two normalized distributions:

$$\mathcal{G}^{(l)} = \left\| \frac{1}{N_v} \sum_{i=1}^{N_v} \hat{\mathbf{v}}_i - \frac{1}{N_t} \sum_{j=1}^{N_t} \hat{\mathbf{t}}_j \right\|_2. \quad (9)$$

A smaller  $\mathcal{G}^{(l)}$  indicates that the visual and textual representations are more closely aligned in the attention key space at layer  $l$ . Since all vectors lie on the unit hypersphere after normalization,  $\mathcal{G}^{(l)} \in [0, 2]$ .

#### B.4 Additional t-SNE Visualization

Figure 6 presents additional t-SNE visualizations for Qwen3-VL-8B and Qwen2.5-VL-7B on MMMU and MMBench-EN. Across all four model–dataset pairs, the Base model shows a visible separation between visual and text representations, reflecting persistent cross-modal discrepancy in the key space. After fine-tuning with MaLoRA, the two modalities become noticeably closer and more mixed. This qualitative evidence further supports our main conclusion that MaLoRA consistently alleviates cross-modal key-space misalignment across different backbones and benchmarks.

#### B.5 Additional Layer-wise Text-to-Visual Attention Change Analysis

To complement the main-text attention analysis on LLaVA-1.5-7B, Figure 7 further reports the layer-wise relative change in aggregated Text→Visual attention for Qwen3-VL-8B and Qwen2.5-VL-7B after MaLoRA fine-tuning. These results provide additional evidence that the strengthened text-to-visual attention pattern generalizes across different MLLM backbones.

### C Evaluation Prompts

To ensure reproducibility and facilitate future research, we provide here the complete set of prompts used to evaluate our model across all benchmarks. These prompts were consistently applied during inference to maintain fairness and comparability.

#### C.1 General Understanding

```
MMBench-EN
< image >
Question: question
Options:
options
Please select the correct answer from the options above.
```

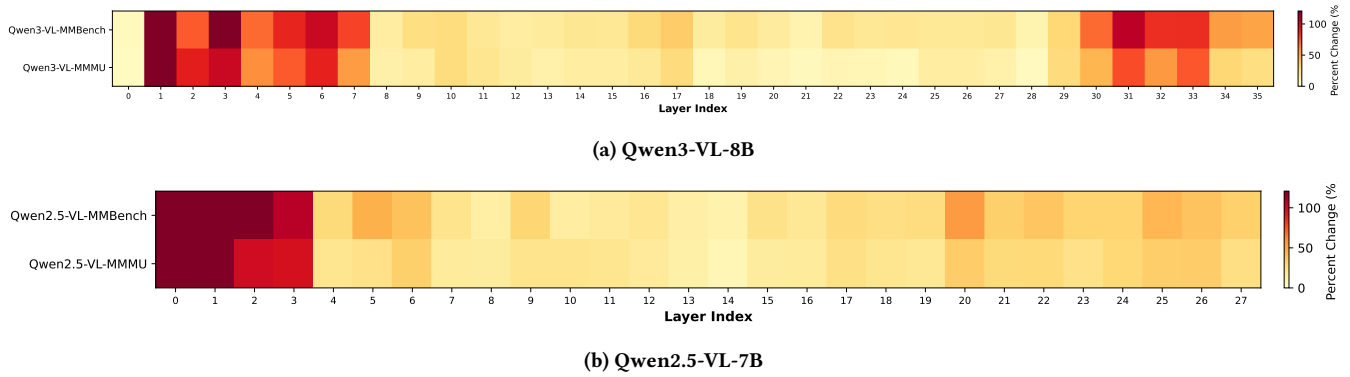


**Figure 7: Layer-wise relative change (%) in aggregated Text→Visual attention after MaLoRA fine-tuning, measured with respect to the corresponding base model on Qwen3-VL-8B and Qwen2.5-VL-7B across MMMU and MMBench. Positive values indicate that textual queries allocate a larger proportion of attention to visual keys after fine-tuning.**

### C.2 Expert Reasoning

MMStar

< image >  
 Question: question  
 Options:  
 options  
 Please select the correct answer from the options above.

SimpleVQA

< image >  
 Question: question  
 Answer the question using a single word or phrase.

### C.3 Math Reasoning

WeMath

< image >  
 Now, we require you to solve a multiple-choice math question. Please briefly describe your thought process and provide the final answer(option).  
 Question: question  
 Option: options  
 Answer the question using a single word or phrase, strictly in the format of A, B, C, D.

DynaMath | MathVision

< image >  
 Question: question  
 Answer the question using a single word or phrase.

## C.4 OCR QA

OCRVQA | TextVQA | ST-VQA

< *image* >

Question: question

Answer the question using a single word or phrase.

## C.5 Structured QA

DocVQA | ChartQA

< *image* >

Question: question

Answer the question using a single word or phrase.

## C.6 GUI Grounding

RICO-ScreenQA

< *image* >

Question: question

Answer the question using a single word or phrase.

You are an impartial evaluator. Given a question, the ground truth answer, and a model's prediction, judge whether the prediction is semantically correct (equivalent to or appropriately conveys the ground truth).

Question: question

Ground Truth Answer: answer

Model Prediction: prediction

Is the model's prediction correct? Answer with ONLY "YES" or "NO". Answer:

## C.7 Domain-Specific

RSVQA

< *image* >

Question: question

Answer the question using a single word or phrase.

VQA-RAD

< *image* >

Question: question

Answer the question using a single word or phrase.